Supporting Information

Amorphous/Crystalline Heterostructure of NiFe (Oxy)hydroxides for Efficient Oxygen Evolution and Urea Oxidation

Tianshan Song,[a] Hui Xue,[*a] Jing Sun,[a] Niankun Guo,[a] Jiawen Sun,[a] Yi-Ru Hao,[a] and Qin Wang[*a]

[a] College of Chemistry and Chemical Engineering, Inner Mongolia University, Hohhot 010021 (P. R. China)

*Corresponding authors: E-mail: qinwang@imu.edu.cn (Q. Wang)

1. Experimental

Materials

$Ni(NO_3)_2 \cdot 6H_2O$, $FeSO_4 \cdot 4H_2O$, $CO(NH_2)_2$, NH_4F, NH_4VO_3, N,N-Dimethylformamide (DMF), and KOH were all purchased from Tianjin Fengchuan chemical reagent technology Ltd. IrO_2 was purchased from Aladdin. Pt/C (20 ωt.%) was purchased from Johnson Matthey. Deionized water was used to prepare all solutions.

Preparation of NiFe LDH/NF

First, the nickel foam (2 cm × 3 cm) was sequentially ultrasonically cleaned in 3 M HCl, deionized water, and ethanol for 30 min, and dried in an oven at 40 °C. $Ni(NO_3)_2 \cdot 6H_2O$ (0.145 g), $FeSO_4 \cdot 4H_2O$ (0.042 g), $CO(NH_2)_2$ (0.15 g), and NH_4F (0.037 g) were added to a mixture of H_2O (14 mL) and ethanol (2.5 mL) at room temperature under stirring for 30 minutes. The mixed solution was poured into a 20 mL autoclave, and the treated nickel foam (NF) was immersed in the solution. The autoclave was kept at 120 °C for 8 hours. After cooling down to room temperature, rinsed with water and ethanol several times, and dried in a vacuum oven at 60 °C.

Preparation of V_x-NiFe LDH/NF

Typically, 5 mg, 10 mg, 15 mg, 20 mg, and 30 mg of NH_4VO_3 and 15 mL of DMF were mixed by sonication for 30 minutes. Pouring the mixed solution into a 20 mL autoclave and immersing the prepared NiFe LDH/NF in the above solution for 8 h at 160 °C. Naturally cooled to room temperature, the samples were rinsed with ethanol and deionized water and dried in a vacuum oven at 60 °C. The samples were named as $V_{0.5}$-NiFe LDH, V-NiFe LDH, $V_{1.5}$-NiFe LDH, V_2-NiFe LDH, and V_3-NiFe LDH, respectively.

Preparation of IrO_2/NF

The 10 mg of IrO_2 and 10 mg of graphene were added to a mixed solution of 20 microliters of Nafion (5%), 100 microliters of anhydrous ethanol solution, and 880 microliters of deionized water to form ink. Then, the 10 microliters of ink were evenly spread on the NF (Geometric Area: 0.25 cm^2).

Preparation of Pt/C (20 ωt.%)/NF

The 10 mg of Pt/C (20 ωt.%) was added to a mixed solution of 20 microliters of Nafion

(5%), 100 microliters of anhydrous ethanol solution, and 880 microliters of deionized water to form ink. Then, the 10 microliters of ink were evenly spread on the NF (Geometric Area: 0.25 cm^2).

2. Material characterization

The crystallinity and crystal structure of the synthesized catalysts are characterized by powder X-ray diffraction instrumentation. The instrument model used is the PAN analytical Empyrean XRD system. X-ray photoelectron spectroscopy (XPS) is applied to characterize the element valence, surface composition, and relative content of each element of the synthesized catalyst. The instrument model used is the XSAM800 photoelectron spectrometer. The scanning electron microscopy (SEM) is performed on a JEOLJSM 6700-F scanning electron microscope. The transmission electron microscope (TEM) and high-resolution transmission electron microscope (HRTEM) images are taken on the JEM-2010 transmission electron microscope system.

3. Electrochemical measurements

Electrochemistry is tested in a typical three-electrode system. The synthesized catalyst is used as the working electrode, the carbon rod is used as the counter electrode, and the Hg/HgO electrode is used as the reference electrode (CHI 760E, Inc. Shanghai). The electrocatalytic activity of OER and water electrolysis are tested by using linear scanning voltammetry (LSV) at room temperature at a scan rate of 5 mV s^{-1} in 1.0 M KOH and corrected for the automatic iR compensation (90%). The electrocatalytic activity of UOR and urea electrolysis are tested by using linear scanning voltammetry (LSV) at room temperature at a scan rate of 5 mV s^{-1} in 1.0 M KOH and 0.5 M urea. EIS data are recorded at open-circuit potentials. Stability is measured by cyclic voltammetry, amperometric i-t curve, and chronopotentiometry. The electrochemical double layer capacitance (C_{dl}) is also determined by cyclic voltammetry (CV). The electrochemically active surface area can be assessed by the slope of the charge current versus the scan rate curve, which is proportional to C_{dl}. All potentials in the article have been converted to hydrogen electrodes ($E_{RHE} = 0.059*pH + E^0_{(Hg/HgO)} + E_{(Hg/HgO)}$). The Faraday efficiency is measured by comparing the experimentally measured and theoretically calculated amount of gas. The Faraday yield is calculated from the total

amount of oxygen produced (n_{O_2}: mmol) and the total amount of charge Q (C) passing through the cell. Suppose four electrons are required to produce O_2 molecule, the faradaic efficiency = $4F \times \frac{n_{O_2}}{Q} = 4F \times n_{O_2} \times 10/t$, where Q = t × 0.1 (C), F is the Faraday constant, and t represents the time (s) for the test time. The overall quantity of oxygen produced during the test is calculated by means of drainage.

4. Computational methods

We have used the firstness principle [1,2] to perform all density generalized function theory (DFT) calculations in the generalized gradient approximation (GGA) using the PBE [3] formulation. We chose the projection augmentation wave (PAW) potential [4,5] to describe the ion nuclei and used a plane wave basis set with a kinetic energy cut-off of 520ev to consider the valence electrons. A Gaussian smearing method using a width of 0.05 eV allows partial occupation of the Kohn-Sham orbitals. When the energy change is less than 10 ~ 6 eV, the electron energy is considered to be self-consistent. The geometric optimization is considered to converge when the force change is less than 0.05 eV/Å. The vacuum spacing perpendicular to the structure plane is 18 Å. The Brillouin zone integration is performed using a curved structure with 2 × 2 × 1 Monkhorst packet K-point sampling. Finally, the adsorption energy Eads was calculated as Eads= E_{ad}/sub -E_{ad} -E_{sub}, where $E_{ad/sub}$, E_{ad}, and E_{sub} are the optimized adsorbent/substrate system, the adsorbent in the structure and the clean substrate respectively. The free energy is calculated as follows:

$$G = E + ZPE - TS$$

where G, E, ZPE, and TS (300K) are the free energy, total energy from DFT calculations, zero point energy, and entropic contributions, respectively.

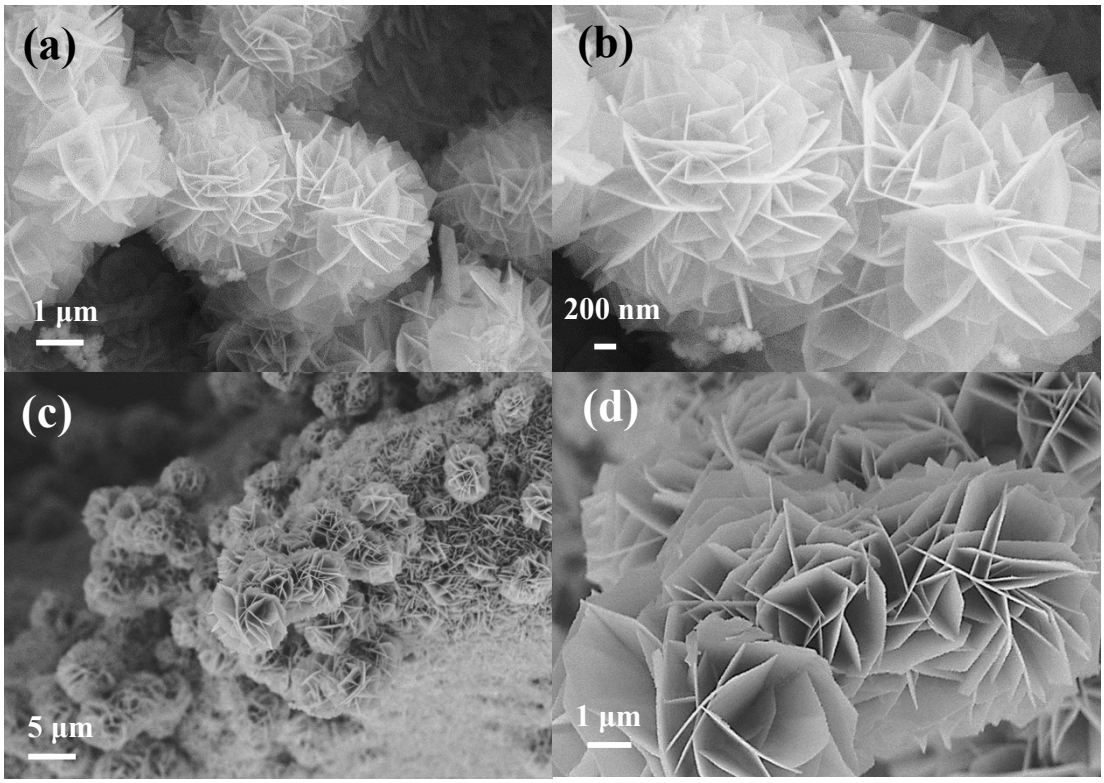

Fig. S1. SEM images with different magnifications of (a, b) NiFe LDH and (c, d) V-NiFe LDH.

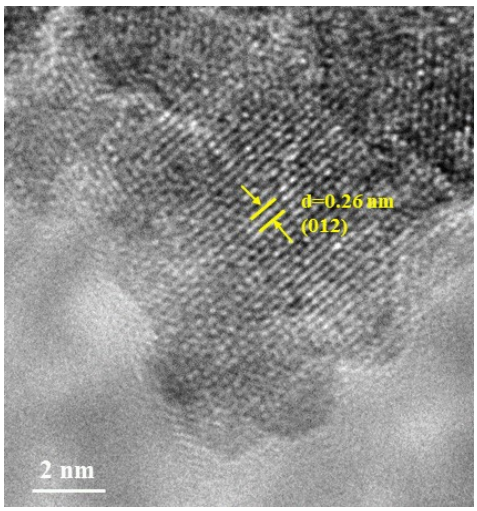

Fig. S2. HRTEM image of V-NiFe LDH.

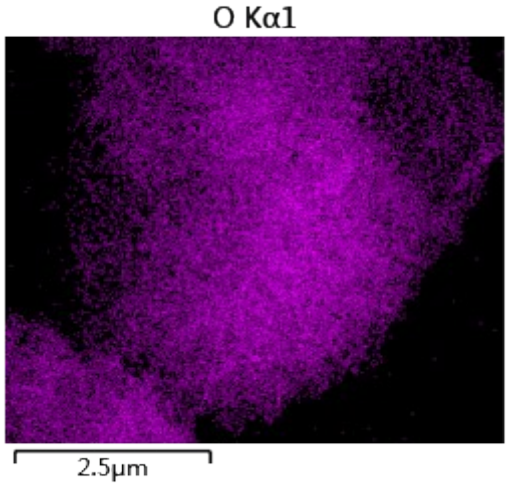

Fig. S3. Oxygen elemental mapping of V-NiFe LDH.

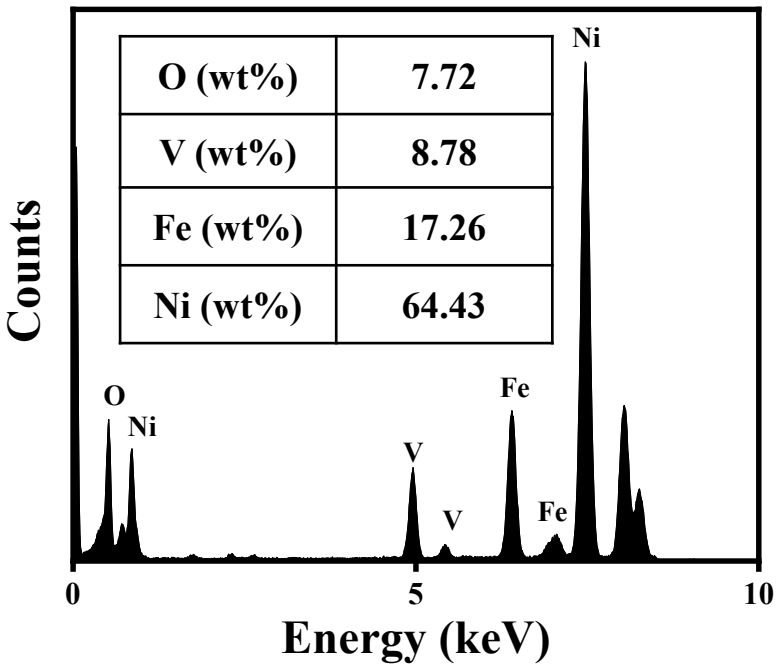

Fig. S4. EDS spectrum of V-NiFe LDH.

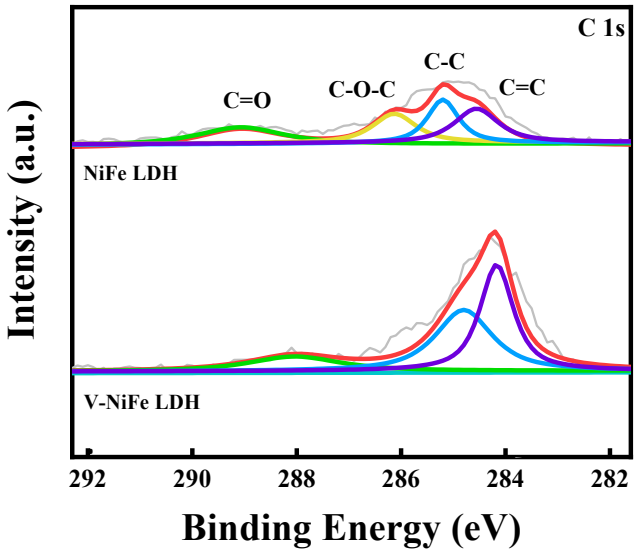

Fig. S5. XPS spectra of NiFe LDH and V-NiFe LDH for C 1s.

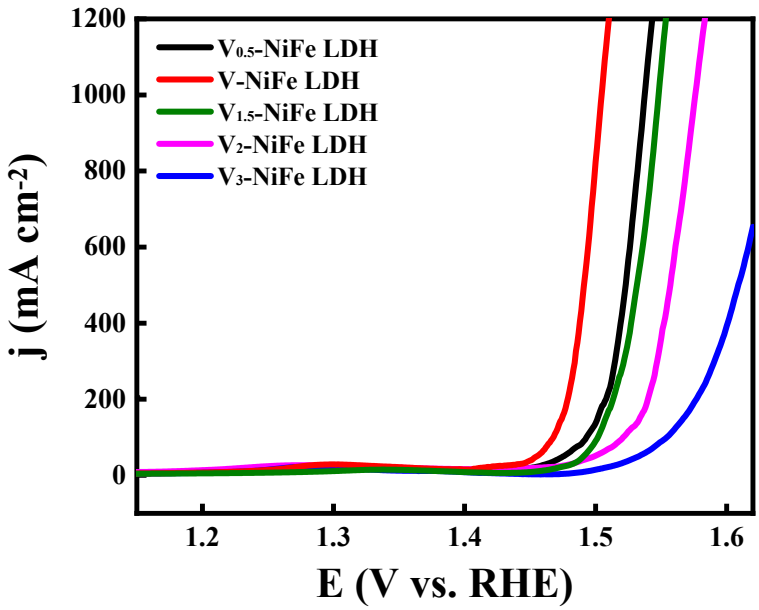

Fig. S6. OER polarization curves of catalysts prepared under doping amounts.

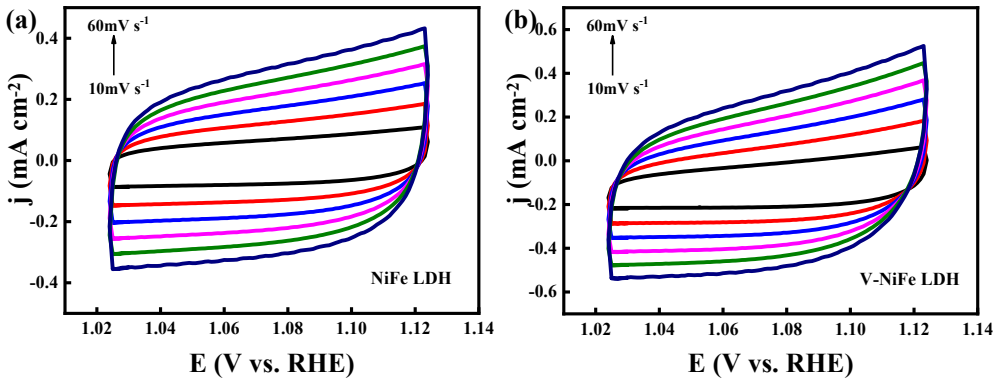

Fig. S7. (a, b) CV curves under different scanning speeds of NiFe LDH and V-NiFe LDH in 1.0 M KOH solution for OER.

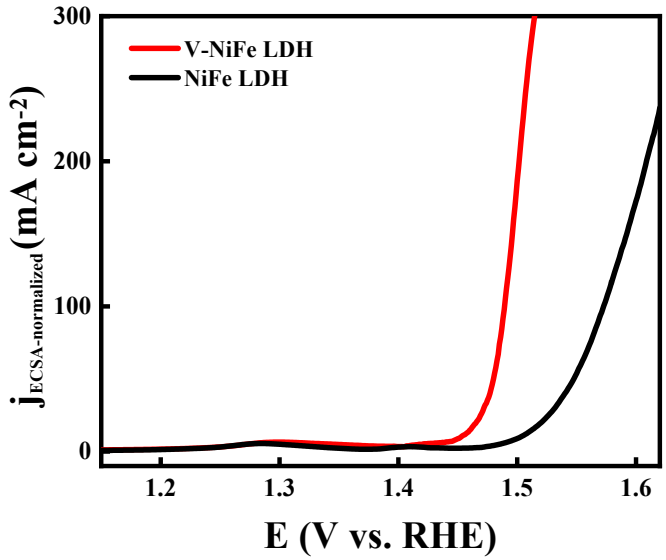

Fig. S8. LSV curves of different catalysts normalized by ECSA in 1.0 M KOH solution for OER.

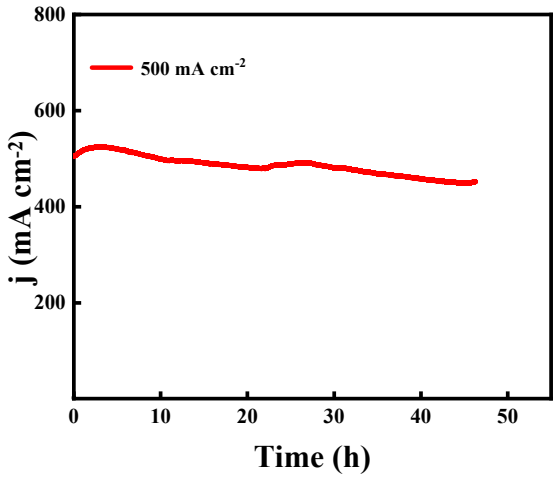

Fig. S9. Potentiostatic tests of V-NiFe LDH at 500 mA cm^{-2}.

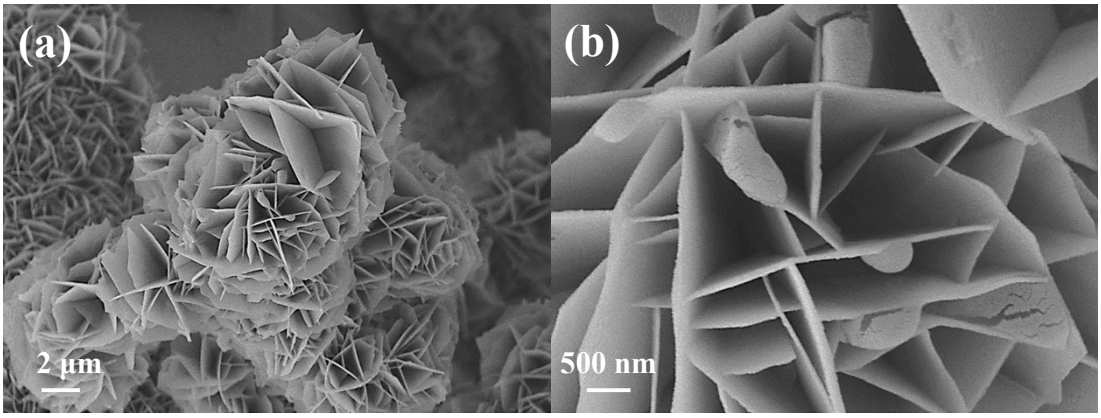

Fig. S10. SEM images of V-NiFe LDH catalysts after 2000 cycles test for OER.

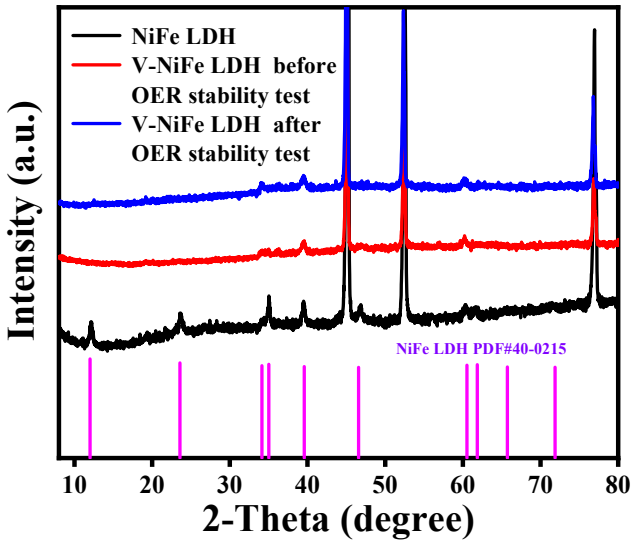

Fig. S11. XRD of the V-NiFe LDH before and after the OER stability test.

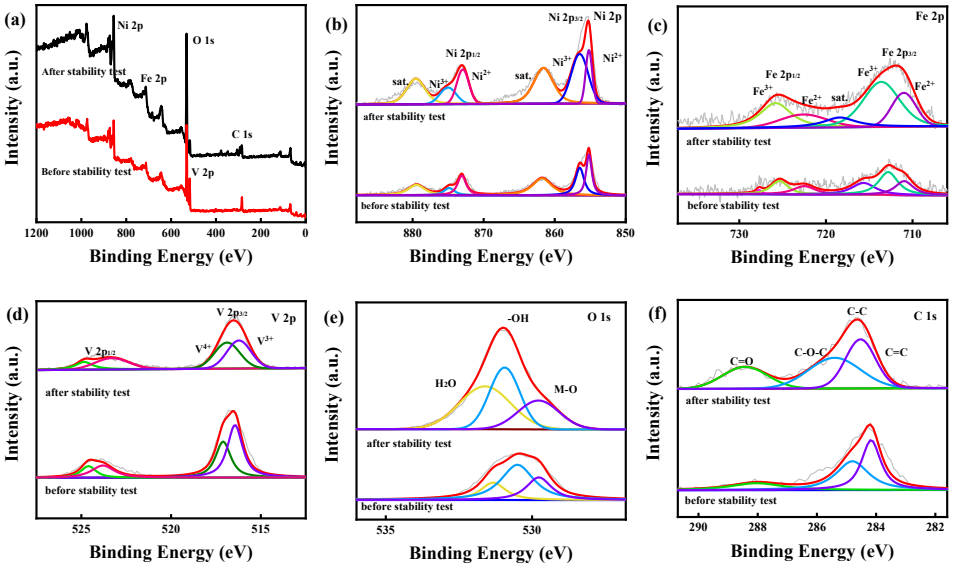

Fig. S12. XPS of the V-NiFe LDH before and after the OER stability test.

The SEM, XRD, and XPS of the V-NiFe LDH after the OER stability test have been measured. As shown in Fig. S10, SEM results reveal that the V-NiFe LDH still maintains the flower cluster-like structure after 2000 consecutive CV cycles. By comparing the XRD patterns of the catalysts before and after OER, it can be seen that the crystalline structure of the catalysts has not changed (Fig. S11). The surface element valence state of the catalyst after OER was studied by XPS test. In Fig. S12a, the elements of Ni, Fe, V, C, and O can be detected. It is noteworthy that the signals of the high valence peaks of Ni, Fe, and V were all enhanced after the stability test, probably due to the oxidation of the anodic potential (Fig. S12b-12d). At the same time, the content of hydroxy-oxygen increases, indicating the existence of activated lattice oxygen in the OER process (Fig. S12e).[6] There were no significant changes in the C 1s region (Fig. S12f).

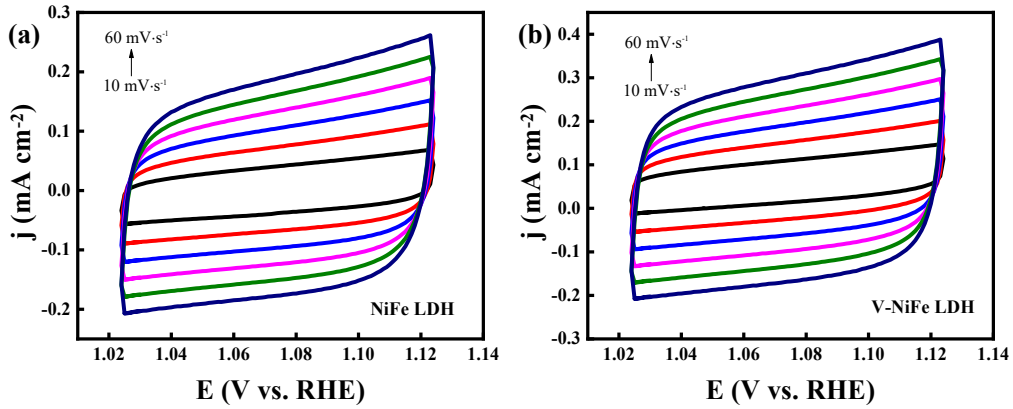

Fig. S13. (a, b) CV curves under different scanning speeds of NiFe LDH and V-NiFe LDH in 1.0 M KOH and 0.5 M urea solution for UOR.

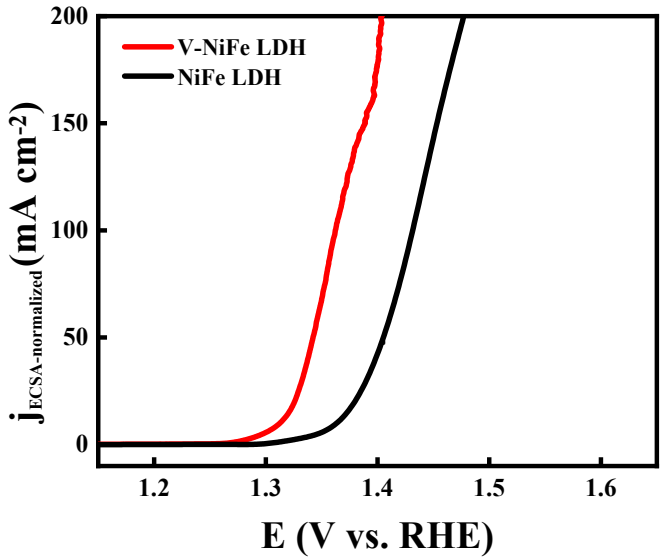

Fig. S14. LSV curves of different catalysts normalized by ECSA in 0.5 M urea and 1.0 M KOH solution for UOR.

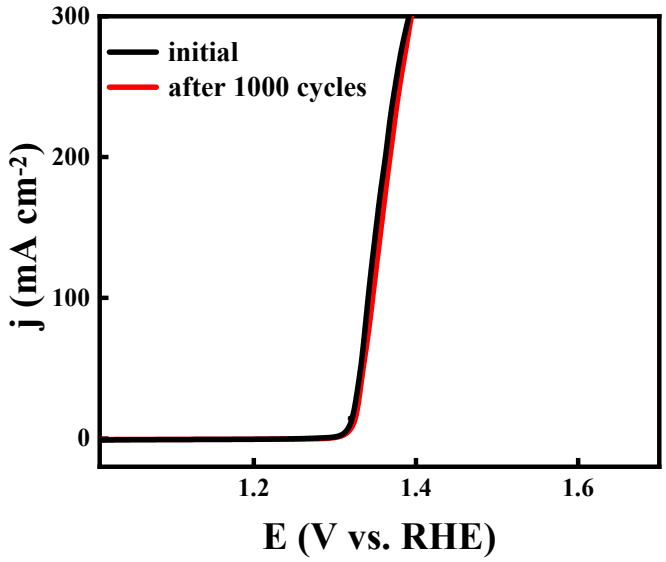

Fig. S15. LSV curves of V-NiFe LDH before and after 1000 cycles for UOR.

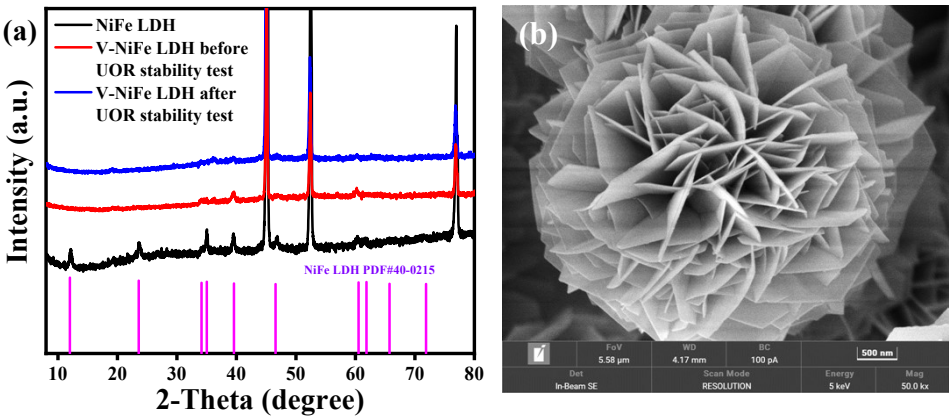

Fig. S16. (a) XRD and (b) SEM of the V-NiFe LDH after the UOR stability test.

In Fig. S16a, there was no significant change in XRD after the stability test, indicating that the catalyst crystalline structure did not change significantly. It can be seen from the SEM image in Fig. S16b that the V-NiFe LDH still maintains good structural integrity after the UOR stability test.

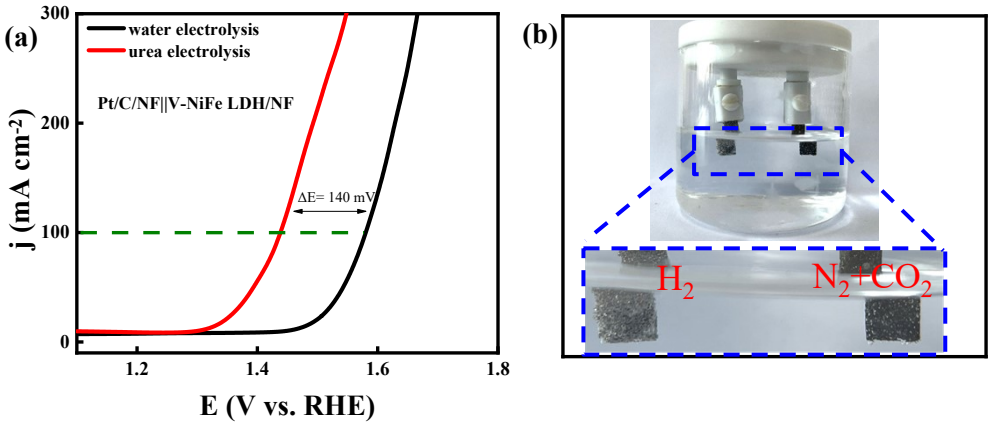

Fig. S17. (a) LSV curves for overall urea electrolysis and water splitting, and (b) the digital photograph of H_2, N_2, and CO_2 bubbles evolving from the electrodes of the urea electrolyzer.

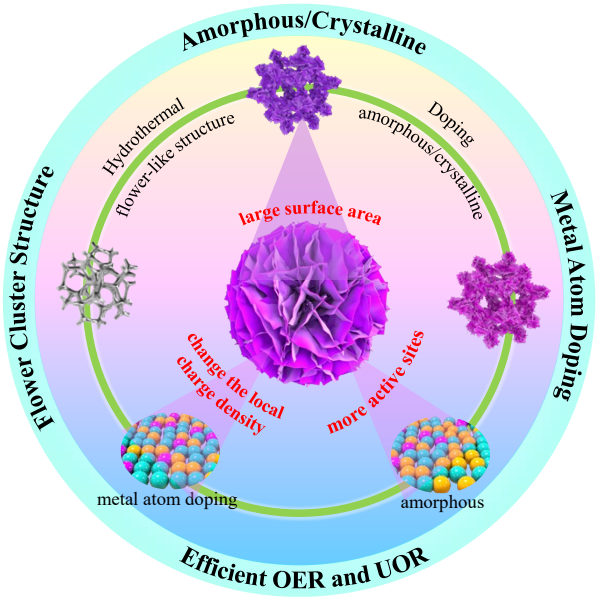

Fig. S18. Schematic diagram of catalytic performance over V-NiFe LDH.

Table S1. The atomic percentage of different elements in various catalysts.

Catalyst	C (at.%)	O (at.%)	V (at.%)	Fe (at.%)	Ni (at.%)
NiFe LDH	18.57	53.04	----	7.2	21.19
V-NiFe LDH	23.34	50.18	3.1	7.01	16.37

Table S2. Summary of representative catalysts that have been recently reported in an alkaline medium of OER.

Catalyst	η (mV)@j (mA cm^{-2})	Substrate	Reference
V-NiFe LDH	230@100	NF	This work
NiFeCo-LDH/CF	**249@10**	**CF**	*Small,* 2020, 16, 2002426
Fe-NiO/NiS_2	**270@10**	**CFP**	*Angew. Chem. Int. Ed.,* 2022, e202207217
$Fe_{0.5}Co_{0.5}OOH$	**250@100**	**CFC**	*Appl. Catal. B,* 2022, 304, 120986
FeNiW-LDH	**250@100**	**FF**	*Nano Energy,* 2021, 80, 105540
NiCe@NiFe/NF-N	**254@100**	**NF**	*Appl. Catal. B,* 2020, 260, 118199
Fe-NiO-Ni CHNAs	**260@100***	**NF**	Appl. Catal. B, 2021, 285, 119809
NiFe LDH	**260@100**	**NF**	*Adv. Mater.,* 2019, 31, 1903909
fcc-NiFe@NC	**263@100**	**CC**	*Angew. Chem. Int. Ed.,* 2019, 58, 6099-6103
CoVFeN@NF	**264@100**	**NF**	*Adv. Energy Mater*., 2020, 10, 2002464
NiMoN@NiFeN	**277@100**	**NF**	*Nat. Commun.*, 2019, 10, 5106
β-$Ni(OH)_2$	**278@100**	**NF**	*ACS Energy Lett.,* 2019, 4, 622-628
FeOOH(Se)/IF	**287@100**	**FF**	*J. Am. Chem. Soc.,* 2019, 141, 7005-7013
V-CoP	**290@100***	**NF**	*Adv. Energy Mater*., 2021, 11, 2101758
(Fe, Co) OOH	**290@100**	**NF**	*Adv. Mater.,* 2022, 34, *2200270*
Ni-Fe LDH DSNCs	**290@100***	**CP**	*Adv. Mater.,* 2020, 32, 1906432
$(Ni_2Co_1)_{0.925}Fe_{0.075}$-MOF-NF	**300@100***	**NF**	*Adv. Mater.,* 2019, 31, 1901139
CoFe-PBA NS@NF	**310@100***	**NF**	*Nano Energy,* 2020, 68, 104371
$NiFe_{0.5}Sn$-A	**310@100***	**CC**	*Adv. Sci.,* 2020, *7*, 1903777
Ni(Fe)OOH	**310@100***	**NF**	*Nano Res.,* 2021, 14, 4528-4533
γ-FeOOH NAs	**316@100**	**NF**	*Adv. Mater.,* 2021, 33, 2005587
FeOOH/Ni_3N	**320@100***	**CC**	Appl. Catal. B, 2020, 269, 118600

CoOOH NAs/CFC	**320@100***	**CFC**	*ACS Catal.,* 2021, 11, 6104-6112
FeCoNi-ATNs/NF	**330@100**	**NF**	*Adv. Energy Mater*., 2019, 9, 1901312
Co@N-CS/N-HCP@CC	**330@100***	**CC**	*Adv. Energy Mater.,* 2019, 9, 1803918
Ni SAs@S/N-CMF	**360@100***	**CP**	10.1002/adma.202203442
$NiCo_2S_4$	**370@100***	**NF**	*Adv. Funct. Mater.,* **2019**, *29*, 1807031
NiFe LDH/NiS	**386@100**	**NF**	*Adv. Energy Mater*., 2021, 11, 2102353
CoN_x@GDY NS/NF	**420@100***	**NF**	*Nano Energy,* 2019, 59, 591-597
NW-$MnCo_2O_4$/GDY	482@100	CC	*Adv. Funct. Mater.,* 2021, 32, 2107179
V-CoP_2/CC	498@100	CC	*Angew. Chem. Int. Ed.,* 2022, e202116233

Note: NF: Ni foam; FF: Fe foam; CC: carbon cloth; CFC: carbon fiber cloth; CP: carbon paper; CFP: carbon fiber paper; * Value calculated from the curve shown in the reference.

Table S3. Summary of representative catalysts that have been recently reported in alkaline medium of UOR.

Catalyst	η (V)@j (mA cm^{-2})	Substrate	Reference
V-NiFe LDH	1.33@100	NF	This work
$Ni_2Fe(CN)_6$	1.35@100	NF	*Nat. Energy,* 2021, 6, 904-912
$NiSe_2$-$NiMoO_4$/NF	1.35@100*	NF	*Chem. Eng. J.,* 2022, 449, 137791
CoMn/$CoMn_2O_4$	1.36@100	NF	*Adv. Funct. Mater.,* 2020, 30, 2000556
Ni_3N/$Ni_{0.2}Mo_{0.8}N$	1.366@100	NF	*Chem. Eng. J.,* 2021, 409, 128240
NiS/MoS_2@CC	1.38@100*	CC	*Chem. Eng. J.*, 2022, 443, 136321
P-Mo-$Ni(OH)_2$ NSAs	1.39@100	NF	*Appl. Catal. B,* 2020, 260, 118154
Ni/FeOOH	1.4@100	NF	*Chem. Commun.,* 2020, 56, 14713
$Ni_{0.9}Fe_{0.1}O_x$	1.4@100	CFP	*Chem. Commun.*, 2019, 55, 6555
Ni-Mo nanotube	1.41@100*	NF	*Nano Energy,* 2019, 60, 894-902
O-NiMoP/NF	1.41@100	NF	*Adv. Funct. Mater.,* 2021, 31, 2104951
a-$Ni(OH)_2$	1.41@100	NF	*J. Mater. Chem. A*, 2019, 7, 13577
CoFeCr LDH	1.41@100	NF	*Appl. Catal B*, 2020, 272, 118959
Fe-Ni_3S_2@$FeNi_3$	1.42@100*	NFF	*Chem. Eng. J.,* 2020, 396, 125315
Ni-S-Se/NF	1.42@100	NF	*Nano Energy*, 2021, 81, 105605
Mo-Co-S-Se	1.42@100	CC	*ACS Sustain. Chem. Eng.,* 2019, 7, 16577
NF/MiMoO-Ar	1.42@100	NF	*Energy Environ. Sci.,* 2018, 11, 1890
NiS@Ni_3S_2/$NiMoO_4$	1.45@100*	NF	*J. Mater. Chem. A,* 2020, 8, 18055
Ni-DMAP-2/NF	1.45@100	NF	*Mater. Today Energy,* 2022, 27, 101024
NF-Ni_2P-Fe_2P	1.46@100	NF	*J. Colloid Interface Sci.,* 2019, 541, 279
NiF_3/Ni_2P@CC	1.53@100*	CC	*Chem. Eng. J.*, 2022, 427, 130865
NiCoP	1.55@100	CC	*J. Mater. Chem. A*, 2019, 7, 9078

Note: NF: Ni foam; FF: Fe foam; CC: carbon cloth; CFC: carbon fiber cloth; CP: carbon paper; CFP: carbon fiber paper; NFF: NiFe foam; * Value calculated from the curve shown in the reference.

References

1. G. Kresse and J. Furthmüller, Efficient Iterative Schemes for Ab Initio Total-Energy Calculations Using a Plane-Wave Basis Set. Phys. Rev. B 1996, 54, 11169-11186.

2. J. P. Perdew, K. Burke and Ernzerhof, M. Generalized Gradient Approximation Made Simple. Phys. Rev. Lett. 1996, 77, 3865-3868.

3. G. Kresse and D. Joubert, From Ultrasoft Pseudopotentials to the Projector Augmented-Wave Method. Phys. Rev. B 1999, 59, 1758-1775.

4. P. E. Blöchl, Projector Augmented-Wave Method. Phys. Rev. B 1994, 50, 17953-17979.

5. S. Grimme, J. Antony, S. Ehrlich and H. J. Krieg, Chem. Phys. 2010, 132, 1541.

6. S.Z. Shao, Q. Zhu, Y. Sun, Y. Zhang, Y.L. Jiang and el at. Adv. Mater. 2022, 34, 2110172.